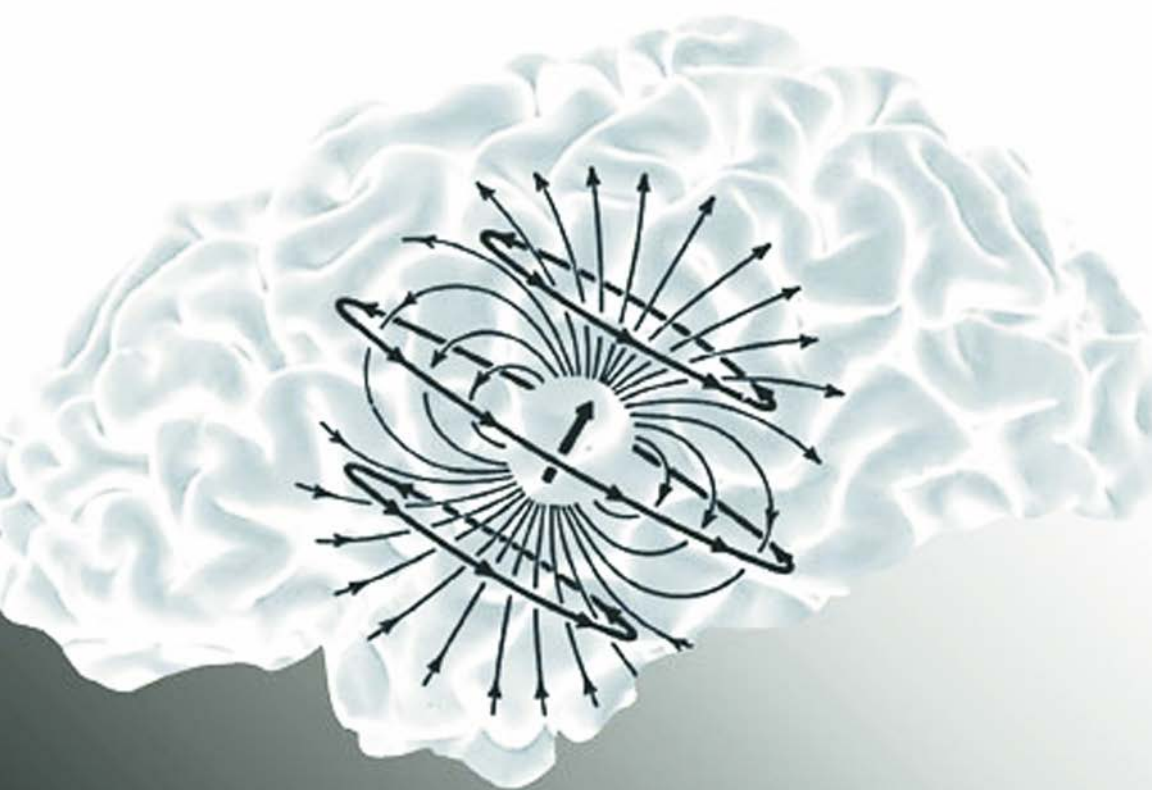


MAGNETIC
SOURCE IMAGING
OF THE
HUMAN BRAIN



EDITED BY

ZHONG-LIN LU • LLOYD KAUFMAN

Magnetic Source Imaging of the Human Brain

Magnetic Source Imaging of the Human Brain

Edited by

Zhong-Lin Lu

University of Southern California

Lloyd Kaufman

New York University



2003

LAWRENCE ERLBAUM ASSOCIATES, PUBLISHERS

Mahwah, New Jersey

London

This edition published in the Taylor & Francis e-Library, 2011.

To purchase your own copy of this or any of Taylor & Francis or Routledge's collection of thousands of eBooks please go to www.eBookstore.tandf.co.uk.

Copyright © 2003 by Lawrence Erlbaum Associates, Inc.

All rights reserved. No part of this book may be reproduced in any form, by photostat, microform, retrieval system, or any other means, without prior written permission of the publisher.

Lawrence Erlbaum Associates, Inc., Publishers
10 Industrial Avenue
Mahwah, NJ 07430

Cover design by Kathryn Houghtaling Lacey

Library of Congress Cataloging-in-Publication Data

Magnetic source imaging of the human brain/edited by Zhong-Lin Lu,
Lloyd Kaufman,
p. cm.

Includes bibliographical references and index.

ISBN 0-8058-4511-9 (cloth: alk. paper)

ISBN 0-8058-4512-7 (pbk.: alk. paper)

1. Magnetoencephalography. I. Lu, Zhong-Lin. III. Kaufman, Lloyd.

RC386.6.M36 M34 2003

616.8'047548-dc21

2002029734

CIP

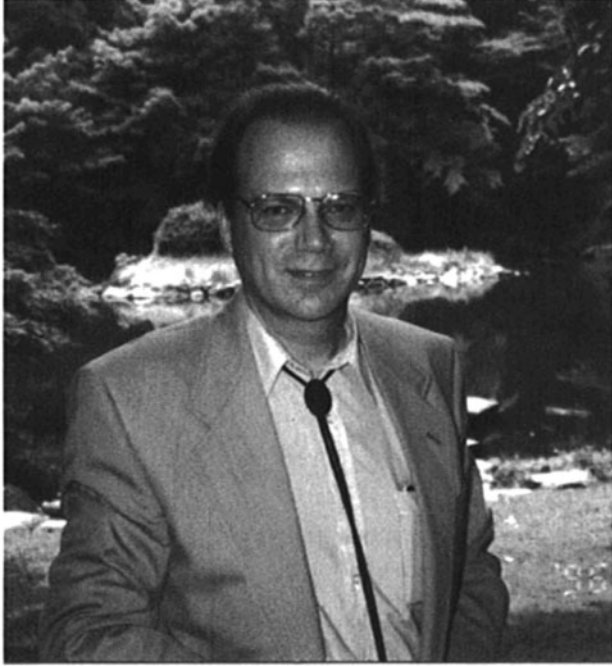
ISBN 1-4106-0917-0 Master e-book ISBN

Contents

Preface	ix
1 Basics of Neuromagnetism and Magnetic Source Imaging <i>Lloyd Kaufman and Zhong-Lin Lu</i>	1
2 Toward Understanding the Physiological Origins of Neuromagnetic Signals <i>Yoshio Okada</i>	43
3 Forward Problem Solution of Magnetic Source Imaging <i>N.G.Gençer, C.E.Acar, and I.O.Tanzer</i>	77
4 Magnetic Source Imaging: Search for Inverse Solutions <i>Jia-Zhu Wang and Lloyd Kaufman</i>	101
5 Techniques for Investigating and Exploiting Nonlinearities in Brain Processes by Recording Responses Evoked by Sensory Stimuli <i>M.P.Regan and D.Regan</i>	135

6	Independent Components of Magnetoencephalography: Localization and Single-Trial Response Onset Detection <i>Akaysha C.Tang and Barak A.Pearlmutter</i>	159
7	Toward Noise-Immune Magnetoencephalography Instrumentation <i>J.Vrba, S.E.Robinson, and A.A.Fife</i>	203
8	Full-Sensitivity Biomagnetometers: Sam Williamson's Vision Brought to Life <i>R.T.Johnson, E.C.Hirschkoff and D.S.Buchanan</i>	217
9	From 1- to 306-Channel Magnetoencephalography in 15 Years: Highlights of Neuromagnetic Brain Research in Finland <i>Olli V.Lounasmaa and Riitta Hari</i>	231
10	Magnetoencephalography: From Pioneering Studies to Functional Brain Imaging <i>Cosimo Del Gratta and Gian Luca Romani</i>	243
11	Optical Imaging of Brain Function and the Relation Between Neuronal Activity and Hemodynamics in Health and Disease <i>Edward L.Maclin</i>	259
12	High-Frequency Oscillations From the Human Somatosensory Cortex: The Interneuron Hypothesis <i>Isao Hashimoto</i>	281
13	Measuring Sensory Memory: Magnetoencephalography Habituation and Psychophysics <i>Zhong-Lin Lu and George Sperling</i>	319

14 Clinical Applications of Brain Magnetic Source Imaging	
<i>Juergen B. Vieth, Helmut Kober, Oliver Ganslandt, Martin Möller, and Kyousuke Kamada</i>	343
Epilogue: Samuel J. Williamson	
<i>Peter Levy and Lloyd Kaufman</i>	365
Author Index	377
Subject Index	393



Samuel J. Williamson at the Sanshiro Pond, University of Tokyo, July, 1996
(photo courtesy of Professor Shoogo Ueno).

Preface

Very faint magnetic fields are now routinely detected outside the human scalp. These fields result from flow of ionic currents within the neurons of the brain and are undistorted by the intervening skull and other tissues. They were first detected more than 25 years ago, and the technology associated with these *neuromagnetic* fields has since grown enormously. The first superconducting devices used to measure the field detected it at a single point in space outside the head. Today hundreds of exquisitely sensitive devices operating at the temperature of liquid helium measure the field at many places at once, thus making it possible to determine the configuration of neuronal currents that give rise to the detected fields. These currents vary with voluntary motor activity, sensory stimulation, and mental activity of various kinds. They also betray the presence of many pathological states and processes. Properly interpreted, the *magnetoencephalogram* is a functional imaging modality that enables a scientist or clinician to literally view the workings of the brain with a temporal resolution measured in milliseconds. Logically this *magnetic source imaging* (MSI) is an ideal complement to functional magnetic resonance imaging (MRI), positron emission tomography, and other functional imaging modalities. It is surprising that this is not yet widely recognized.

Perhaps the lack of recognition is related to the pre-eminent role played by low-temperature physics in much of the early literature and the abstract concepts underlying more recent efforts to convert measures of the extracranial magnetic field to images of the brain in action. Insufficient attention has been paid to communicating the essence of MSI to a wider scientific audience. It seems fairly easy to grasp the significance of readily interpreted functional MRI images colored or shaded to reveal the regions of the brain that were

apparently more or less active during the performance of some mental task. By contrast, current dipole moments, current source distributions, and isofield contour plots seem to communicate little to the unprepared reader. This situation cannot be remedied by referring interested scientists to an extensive but highly specialized literature, written in a language recognized by a relatively few specialists. Hence, this book is designed to acquaint serious students and scientists with MSI.

On September 24, 1999, a group of prominent scientists gathered to honor Professor Samuel J. Williamson, one of the most influential early pioneers of MSI. This conference at New York University was entitled “*Neuromagnetism at the Millennium.*” The speakers were physicists, engineers, physicians, cognitive scientists, neural scientists, and psychologists. They discussed the history of the field as well as the current state of the art. Some dealt with near-term and therefore predictable future developments of the technology. All in attendance agreed that a similarly full treatment in the form of a book would go a long way toward filling the need described earlier.

Although this book originated as the proceedings of a conference, it has been organized and expanded to cover the field in a coherent manner. We solicited new chapters from outstanding scholars and prepared an introductory tutorial chapter. Contributors include distinguished scientists from many different countries, including Canada, Japan, Finland, Germany, Italy, the Netherlands, Turkey and, of course, the United States. Some are widely known outside the field of MSI. The list of authors includes many who are members of their nation’s academies of science, recipients of prestigious scientific prizes, and authors of some of the most widely cited articles in their own special fields. Most of the authors have made pioneering contributions to the field of MSI and, obviously, all recognize the potential importance of this field. We are extremely pleased that this distinguished group agreed to participate in the conference to honor Professor Williamson and to contribute chapters to this book.

This book is self-contained. It covers MSI from beginning to end. The first sections review the principles and methodology, and the remainder reviews the results obtained by the most important laboratories worldwide. As indicated earlier, to prepare the readers, we wrote chapter 1 to introduce the field and to provide a framework for the rest of the book. We think this volume would be a suitable textbook for upper-level undergraduate and graduate courses on brain imaging (in fact, several authors have been using their own chapters in graduate courses). However, the book is primarily intended for scientists, graduate and postdoctoral students working in areas of biomagnetism, brain imaging, and cognitive neuroscience.

All the contributors and many other people have given us a great deal of help in producing this book. In particular, we thank George Sperling for his advice and Bill Webber for his encouragement and cooperation. We are very grateful to Sara Scudder and Janet Lincoln for their careful and thoughtful assistance. We also thank New York University and its Department of Physics for sponsoring the conference that led to this book. Biomagnetic Technologies, Inc. (now 4D Neuromagnetic Imaging, Inc.) provided some additional financial support. We are especially grateful to those who came from as far away as Finland, Japan, Italy, and many other places to make their contributions. These many scholars came because of Samuel J. Williamson's scientific and personal contributions to their work. We dedicate this book to Sam Williamson, a true pioneer who played a major role in creating the field of MSI of the human brain.

—*Zhong-Lin Lu, Irvine, California*

—*Lloyd Kaufman, Roslyn Heights, New York*

1

Basics of Neuromagnetism and Magnetic Source Imaging

Lloyd Kaufman
New York University

Zhong-Lin Lu
University of Southern California

This chapter provides an overview of *neuromagnetism*, which is defined as the study of magnetic fields associated with the electrical activity of neurons. Like the other chapters in this volume, this chapter especially emphasizes the magnetic fields generated by the human brain. In view of this emphasis, we introduce the reader to *magnetoencephalography*, a technique that measures the external magnetic field, near the scalp, of the intact human brain. This general overview is designed to help newcomers appreciate the more technical chapters. It provides a relatively nontechnical description of the physical basis of the neuromagnetic field, the different methods used to detect it, and how the magnetoencephalogram complements the *electroencephalogram*. We explain how analysis of MEG data can yield high temporal and reasonable spatial resolution “representations” of current distributions on the cerebral cortex. These magnetic source images complement the other functional imaging modalities. Furthermore, we describe some typical uses of *magnetic source imaging* in medicine and in cognitive neural science. Finally we briefly discuss complementary modes of functional brain imaging; such as *positron emission tomography* and *functional magnetic resonance imaging*, as well as recent attempts to combine multiple imaging modalities to achieve high spatiotemporal resolution functional images of the human brain.

One goal of this chapter is to acquaint readers with areas of research that are awaiting the attention of creative scientists. To achieve this goal, we must make a seemingly esoteric subject accessible. Hence; this chapter does not provide an exhaustive review of the literature; instead? we attempt to elucidate relevant principles, methods, and results in as simple a manner as possible and point the way so that even beginners will recognize opportunities to make advances in the field. The other chapters in this volume cite the relevant literature and describe historical precedents in great detail and can serve as a basis for further study and research. Thus, one of our major goals is to prepare beginners to read these chapters.

THE NEUROGENESIS OF MAGNETOENCEPHALOGRAPHY

In chapter 2 of this volume? Yoshio Okada provides a detailed discussion of how neurons give rise to magnetic fields. In this section we offer a brief and simplified account.

Primary and Volume Currents

Neurotransmitters crossing a synapse produce local changes in the electric potential across the target membrane. This postsynaptic potential tends to be either excitatory or inhibitory; that is, it either reduces or increases the polarization of the target membrane, depending on the nature of the neurotransmitter. The interior resting voltage of the cell is normally negative with respect to its exterior. As the polarization of the membrane is reduced, or even reversed, near the synapse the internal potential of the cell membrane becomes less negative relative to that of more distant regions of the membrane. This difference in potential between one region of the cell's inner wall and that of more distant regions results in current flow. Conversely when the local transmembrane potential is increased (hyperpolarized) so that negativity of the interior of the membrane is greater near the synapse relative to more distant regions; negative ions will tend to flow away from that region toward more distant portions of the cell This intracellular ionic current flow may persist for a relatively long time. The entire neuron can be thought of as a very small battery and a resistor connected to its positive pole. The battery-resistor combination is immersed in a saline solution. Because the solution is a conductor, it completes the circuit between the (positive) end of the resistor and the negative pole of the battery. This allows ionic current

to flow widely throughout the solution from the positive end of the resistor to the opposite (negative) pole of the battery. The positive end of the resistor tends to lose charge as negative ions flow from it into the saline medium. This charge is replaced by ions from within the battery. These negative ions inside the battery are replenished in turn by inflowing ions from the medium. As a consequence; charge is conserved, because there is a continuous flow of current around the complete battery-resistor-medium circuit. We refer to the intracellular current, within the battery and resistor, as the *primary current*. The primary current represents the ionic currents flowing within elongated processes of neurons, for example, dendrites of pyramidal cells of the cerebral cortex. Alternatively the currents flowing outward from the battery-resistor circuit into the saline solution and inward from that solution toward the circuit's opposite pole are referred to as the *volume currents*. These currents correspond to extracellular currents that flow within the cerebrospinal fluid throughout the intracranial space. Because the skull has very high electric resistance, volume currents flow through the orbits of the eyes and other openings in the skull into the scalp, where they create the potential differences that underlie the electroencephalogram (EEG). The magnetic fields surrounding the neurons pass undisturbed through the skull to produce the magnetoencephalogram (MEG).

Both the volume currents and the intracellular ionic currents are depicted schematically in Fig. 1.1. In this instance, we assume that the source of the magnetic field \mathbf{B} is a segment of current that is very small relative to the distance at which the field is measured. Hence, it is possible to model it as an *equivalent current dipole* (ECD). Because magnetic fields are superimposable (i.e., they are additive and do not interact with each other), extracranial fields do not arise from a single neuron but actually represent the sum of the fields of many similarly oriented hypercolumns of concurrently active cortical cells.

In Fig. 1.1, $\mathbf{Q} = I \times \vec{L}$, where I is the amplitude of the current and \vec{L} is the length and direction of the current segment. Because the dipole has both direction and strength, \mathbf{Q} is a vector quantity representing the strength of the dipole in ampere-meters (the dipole's *moment*). The volume current also varies in strength and direction. The symbol \mathbf{J}' indicates that the value of the direction and strength of the volume current depends on the position at which it is measured.

All moving electric charges are accompanied by magnetic fields. Because the volume currents are composed of moving electric charges, these too must be accompanied by magnetic fields. However, when the dipole is immersed in an infinitely large volume (or in a finite sphere), the direction

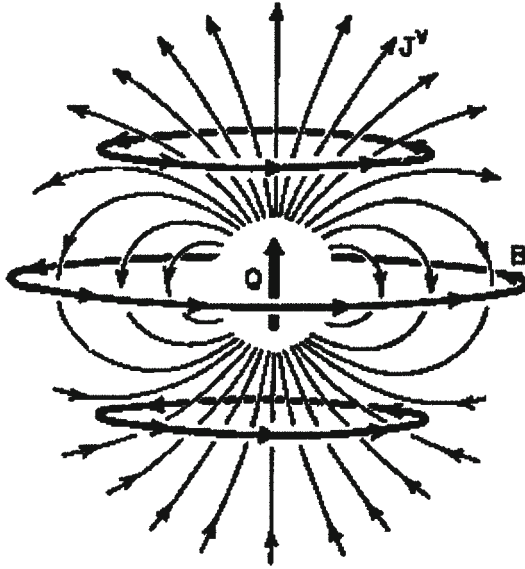


FIG. 1.1. A current dipole immersed in a homogeneous conducting medium. The magnetic field (\mathbf{B}) is due solely to the current dipole (moment= Q), with the volume currents (represented by the thin lines [J^v]) making no contribution to the field.

of the field associated with an ion at one place and time is opposite from that associated with ions at other places at the same time. Therefore, the fields of these oppositely directed moving charges cancel each other out, that is, the sum of the fields of the volume current measured at some distant point is effectively zero. Thus, the field measured at a distance is due solely to the net primary current, which is largely associated with postsynaptic dendritic potential changes.

A distinction is often made between *open-field* and *closed-field* neurons. The latter are so designated because their dendritic trees are approximately symmetrical in three dimensions. Because of their morphological symmetry, these cells are presumed to contribute little to either electric or magnetic fields detected some distance away, because the net electric and magnetic fields produced by symmetric current distributions are zero. For example, basket cells are sometimes described as closed-field cells. On the other hand, pyramidal cells are prototypical open-field neurons, because their apical dendrites incorporate one-dimensional elongated processes. Ionic currents within these dendrites are excellent candidate sources of external fields and potentials. However, one must bear in mind that cell morphology alone does

not determine whether a cell's magnetic field is detectable at a distance. For a cell with a symmetric dendritic tree, there could still be an asymmetric distribution of primary current (e.g., due to asymmetric presynaptic activities) and therefore a field that can be detected at a distance. Thus, although the literature often implies that pyramidal cells are the sole sources of external fields; this claim has not been proved. For example, stellate cells do not have elongated dendrites. They, and not pyramidal cells, are predominant in the visual cortex. Yet some of the strongest MEG (and EEG) signals arise from the visual cortex.

As already noted, the volume currents flowing in the dermis of the scalp create the potential differences that underlie the EEG. Brain tissue and the fluid filling the subarachnoid space are relatively good conductors, especially as compared with the skull, which is highly resistive. These anisotropies in conductivity must be taken into account in attempts to identify the neural sources of scalp-detected potentials (Nunez, 1981). The difficulties in locating neural sources of EEG/event-related potential (ERP) are further compounded by the fact that the skull and other tissues are relatively asymmetrical, so that the paths of flowing volume currents are also asymmetrical. Finally, in measuring the EEG (as well as the ERPs considered later), one must use a reference or ground electrode. This is never a truly indifferent electrode, as it is affected by activity of the brain at regions that may be far from the "active" electrode. One must take this into account in interpreting a pattern of potentials across the scalp. Despite these factors, the EEG is capable of providing vital information regarding the linkage between particular scalp-detected phenomena and underlying process. For example, the presence of the classic spike and wave in the EEG may be diagnostic of epilepsy, even though sometimes it is not possible to accurately determine the location of the lesion responsible for seizures. To take another example, despite early controversy regarding the source of the N100 component of the *auditory-evoked potential* (AEP), this component proved to be a useful candidate for the study of attention.

To summarize, the scalp is "transparent" to magnetic fields (see chap. 2, this volume) but not to the electric potential produced by the brain. This makes interpretation of MEG a much simpler problem than that of EEG. Even though many recent ERP localization methods attempt to take account of these conductivity problems by using sophisticated volume conductor models of the head, ERP source localization is still a very difficult problem. A good example is in the study of N100, a relatively negative voltage peak (component) in the AEP that occurs about 100 msec after the onset of an acoustic stimulus. (In the MEG literature, the magnetic counterpart to N100

is often referred to as *M100*.) The AEP is normally detected at a midline electrode (at the vertex). As explained in chapter 9 of this volume, the sources of this component lie within the auditory cortex of each of two hemispheres. MEG experiments have revealed that at least two (and probably more) sources in each hemisphere underlie N100. The sources in the two hemispheres differ in strength and are affected somewhat differently by attention to tonal stimuli (Curtis, Kaufman, & Williamson, 1988). The many published AEP studies do not report this asymmetry. Similarly auditory evoked fields (AEFs) in response to tones of different pitch have sources that occupy different positions along the auditory cortex. The tonotopic organization of the human auditory cortex was first revealed in MEG experiments (Romani, Williamson, & Kaufman, 1982). The tonotopic organization of the human auditory cortex is described by Cosimo Del Gratta and Gian Luca Romani in chapter 10. Other imaging modalities have confirmed this finding. For example, single photon emission tomography has revealed a similar organization of the human auditory cortex (Ottaviani et al., 1997). Similar findings were obtained using functional magnetic resonance imaging (fMRI; Wessinger, Buonocore; Kussmaul, & Mangun, 1997).

Thus far, even after 20 years, this property of the auditory cortex has not been revealed in any AEP study, although an experiment with indwelling electrodes has confirmed the finding (Liegeois-Chauvel et al., 2001). So, even though the ultimate sources of the AEP and the AEF are the same, the two types of measures (MEG and EEG) differ in certain vital respects. We now make these differences clear.

Effect of Source Orientation

For the present it is useful to represent the sources of the MEG and EEG as equivalent current dipoles. Let us assume that the volume currents associated with an ECD underlie the EEG, and the field surrounding the ECD is a source of the MEG.

Many early MEG studies made the simplifying assumption that the head may be represented by a sphere the radius of which is approximately the same as the radius of curvature of the skull over which neuromagnetic measurements are made. As we shall see, this practice is beginning to give way to one in which more realistic head shapes are used (see chap. 3). For the sake of clarity however, we stay with the older and still widely applied practice.

The sphere in Fig. 1.2a is 20 cm in diameter, and a current dipole is located 4 cm beneath its surface. It is very important to note that the current

dipole is oriented at a right angle to a radius, that is, it is oriented tangentially with respect to the surface of the sphere. In practice, the field is measured simultaneously at many points about the sphere's surface. Each pickup coil of the *neuromagnetometer* used to detect the field is also oriented tangentially with respect to the surface. Therefore, it senses the radial component of the field, not its tangential component. Note that the radial component of the field is associated with the tangential component of the dipole moment; the tangential component of the field is associated with the radial component of the dipole moment. It is customary to project these measurements onto a planar surface, which in this example has an area of $22.4\text{ cm} \times 22.4\text{ cm}$.

The radial component of the field is directed either outward or inward with respect to the surface of the sphere and does not include the component tangential to the surface. The strength of this radial component of the field varies with the place of measurement and is represented by the *isofield contours* shown in Fig. 1.2b. These isofield contours form a typical *dipolar field pattern*. It contains one region where the emerging field is at its maximum and another where the re-entering field is at its maximum. The centers of these regions are labeled *field extrema*. As one moves along a line defining

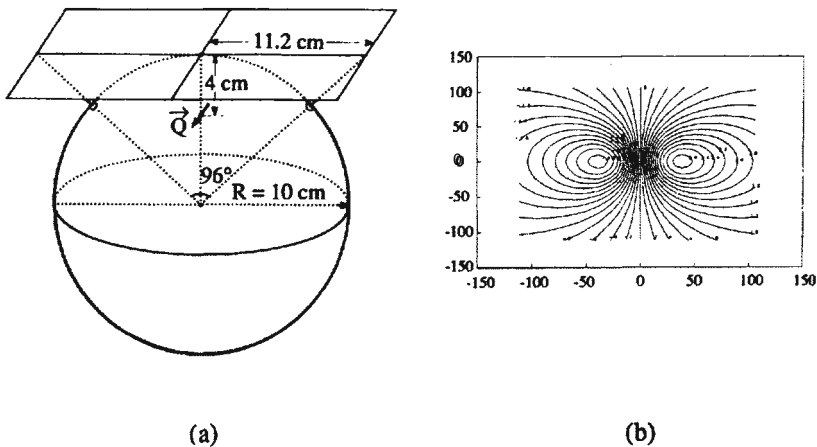


FIG. 1.2. Panel (a): schematic of a current dipole 4 cm beneath the surface of a 10-cm radius sphere. The radial component of the field is projected onto the surface of a rectangle tangential to the sphere. The center of the rectangle is directly over the point dipole. Panel (b): the isofield contour plot on the surface of the rectangle. The contours represent the relative radial field strengths in arbitrary units.

the shortest path connecting these two extrema, a point is reached where the strength of the radial component of the field is zero. This zero point is precisely halfway between the field extrema. Moreover, the ECD lies directly under this point. Because our hypothetical measurements are restricted to the radial component of the field, the radial component has a value of zero halfway between the two extrema. As a matter of fact, the depth of an ECD lying directly beneath this halfway point is easily computed from the distance separating the field extrema on the surface of the scalp and the radius of the sphere that best fits the scalp on which those extrema are found. This insight made it possible to establish the tonotopic progression of sources along the auditory cortex (Romani et al., 1982).

Assuming that an ECD is 4 cm beneath the surface of a 10-cm radius sphere and oriented tangentially with respect to its surface (Fig. 1.2A), the relative strengths of the emerging and re-entering components of the field were computed. The isofield contours of Fig. 1.2B were then plotted. The computation is based on Equations 1.1 and 1.2.

$$\vec{B}_r = \frac{\mu_0}{4\pi} \frac{\vec{Q} \times (\vec{r} - \vec{r}_0)}{|\vec{r} - \vec{r}_0|^3} \tag{1.1}$$

where \vec{B}_r = the field at a point \vec{r} in space, \vec{r}_0 = the vector from the center of the sphere to the dipole, \vec{Q} = the current dipole moment; and μ_0 = the permeability of free space. Because the isofield contours of Fig. 1.2 represent only the strengths of the radial component of the field at the surface of the sphere, that component, \vec{B}_n (\vec{B}_n), is simply the dot product

$$\vec{B}_n = \vec{B} \cdot \vec{r} / |\vec{r}| \tag{1.2}$$

If the dipole shown inside the sphere of Fig. 1.2 were tilted so that it is no longer tangential to the surface of the sphere, it could be described as being composed of two components, one oriented tangentially and the other radially. Ultimately as the tilt increases, the dipole has no tangential component, because it is aligned with a radius extending from the center of the sphere to its surface. As the ECD is tilted from its initial tangential orientation, the dipolar field pattern at the surface simply diminishes in intensity. When the dipole's orientation is entirely radial, no radial field can be detected at the sphere's surface. It is interesting to note that the field pattern does not shift in

position even as its intensity diminishes throughout the time that the dipole is rotating. The dipole would still lie directly beneath the point bisecting the distance between the field extrema. In other words, if the conductive volume is perfectly spherical, then measures at the surface of the sphere are sensitive only to the tangential component of the current dipole moment and not to the radial component of the current dipole moment.

The electric potential distribution across the spherical surface has different properties. As already indicated, the volume currents that accompany the current dipole produce potential differences across the surface of the sphere. These may be represented by *isopotential* contours similar in appearance to the dipolar pattern of the isofield contours described earlier. (In attempts to achieve a more realistic model of the human head, three or four concentric spheres representing layers of different conductivity replace the single sphere shown in Fig. 1.2. These different layers result in a spreading or blurring of the isopotential contours, but it remains essentially dipolar when the underlying dipole is tangential to the scalp.) The most significant difference between the isofield and isopotential contours in this simple example is that the latter are rotated 90° on the projection plane with respect to the former. However, as the dipole is tilted from its tangential orientation, the positions of the isopotential contours shift and become asymmetrical. The potential at the extremum associated with the more distal (deeper) end of the underlying dipole grows weaker, while the extremum associated with the opposite pole (which is closer to the surface) grows stronger. The latter extremum migrates toward a point directly over the dipole, while the opposed extremum moves away from that point. Finally, when the dipole is oriented along a radius of the sphere, there is only one extremum on the surface. Of course, asymmetrical differences in conductivity within the head would result in greater differences between the patterns of isofield and isopotential contours.

The distinction between radial and tangential ECDs is important. For example, if the MEG represents tangential sources and the EEG represents both tangential and radial sources, it may be possible to subtract MEG data from some transform of EEG data and obtain an “image” of the radial sources. It is widely accepted that the radial sources dwell in the gyri of the cortex, while the tangential sources are to be found in the sulci. This could have obvious advantages.

Despite widespread recognition of this possibility one must be circumspect with regard to its actual promise. For one thing, real sources of electric and magnetic fields in the brain are not point current dipoles; they are assemblies of many concurrently active neurons. Lu and Williamson (1991) estimated that the typical cortical area involved in coherent sensory-evoked responses

is about 80–100 mm^2 . A hypercolumn is composed of about 30,000 neurons, and several of these hypercolumns must be active if they are to produce a detectable field or a detectable difference in scalp potential. All neurons are bent, so any hypercolumn, even if it is largely normal to the surface of a gyrus, contains both radial and tangential components. Consequently, neurons in gyri will produce extracranial dipolar field patterns, although these are likely to be very much weaker than if the same arrays of neurons were in the walls of a sulcus. Similarly columns of neurons oriented approximately normal to the surface of a sulcus will have radial as well as tangential components. Hence; neurons in a sulcus may well contribute to the ostensibly “monopolar” isopotential patterns on the scalp associated with radially oriented sources. Hence, with sufficiently sensitive instruments; sources in gyres would be detected in extracranial fields.

Although we emphasize that the skull is not a sphere, some truly remarkable results were achieved with the skull modeled as a best-fitting sphere (e.g., Romani et al., 1982). It is worthwhile to consider why this is the case.

The early assumption that the skull and scalp do not distort magnetic fields is now confirmed. The fields that emerge from and re-enter the skull are not altered by the presence of the skull and scalp (see chap. 2). Hence, one can effectively ignore the physical skull and scalp when measuring the radial component of the neuromagnetic field. Today large arrays of detectors are usually arranged to fit the spherical surface of the tail section of the cryogenic dewars of neuromagnetometers. The fields penetrate this tail section without distortion. The surface of the tail section of the dewar is placed so that it is concentric with a sphere that best fits the head. The skull may not be perfectly concentric with the spherical array of sensors; hence, the measured field may include some contribution by the tangential field component. In effect, this introduces an error in the measured magnitude of the field. However, the position of a virtual current dipole placed at a known location in a model of a head can be determined with an accuracy of about 2 mm (Yamamoto, Williamson, Kaufman, Nicholson, & Llinas, 1988). Apparently, assuming that the head is spherical is not necessarily a major source of error in evaluating MEG data. This is not the case for the EEG, and one should consider this potential mismatch when attempting joint use of EEG and MEG data.

In a real head, a sphere with a particular radius of curvature may be a nearly perfect match to the curvature of the skull lying immediately above a current dipole source. The source may be radially oriented with respect to that particular sphere. However, the radii of curvature of adjacent regions of the skull may be different; hence, the same dipole is not exclusively radial in orientation with respect to those segments of the skull. It is obvious that a

realistic head shape makes the distinction between radially and tangentially oriented dipoles somewhat ambiguous. Therefore, it is important to evaluate how realistic head shapes affect the measured electric and magnetic fields (see chap. 3).

MEASURING THE NEUROMAGNETIC FIELD

Ions flowing within neurons are surrounded by magnetic fields. Thus, intracellular ionic currents result in magnetic fields that surround neurons. Fields of different neurons do not interact with each other. Therefore, the measured field at a point in space is simply the sum of the fields contributed by each neuron. Because the field strength varies inversely with the square of the distance from a small (current dipole) source, a field measured at a point outside the human scalp would reflect the activity of relatively nearby neurons and be largely uncontaminated by fields of very distant neurons. As we shall see, suitably sensitive instruments make it possible to detect such fields of the brain. Thus far we have discussed fields associated with very simple sources, that is, ECDs immersed in a conducting solution enclosed by a nonconducting spherelike skull. Before turning to more realistic situations, we should introduce the methods used to measure the neuromagnetic field.

Fig. 1.3 is a schematic representation of a single-channel system that was used to measure the brain's neuromagnetic field. (It is important to note that existing systems use a very large number of sensors, and the single-channel shown here corresponds to only one of those sensors [see chaps. 7 and 8].) In Fig. 1.3, a magnetic field is shown emerging from one region of a subject's skull and re-entering a nearby region. The isofield contours represent those places where the emerging and re-entering fields have lesser values than the fields at the two extrema. The purpose is to measure the component of the field normal to the scalp at each of many positions.

The fields in question are extremely weak (about 50 femto Tesla), being on the order of 1 billionth the strength of the earth's steady field (=50 micro Tesla), which is weaker than the fields of manmade magnets and motors as well as those associated with vibrating steel building frames and other urban sources of electromagnetic fields. This requires the use of an exquisitely sensitive instrument with a low intrinsic noise level and also capable of discriminating against extraneous magnetic fields. The sensitivity is provided by a device known as a *SQUID* (superconducting *quantum* interference *device*), which operates at the temperature of liquid helium (4.2° K). Fig. 1.3 depicts a SQUID contained within a cryogenic *dewar* where it is immersed

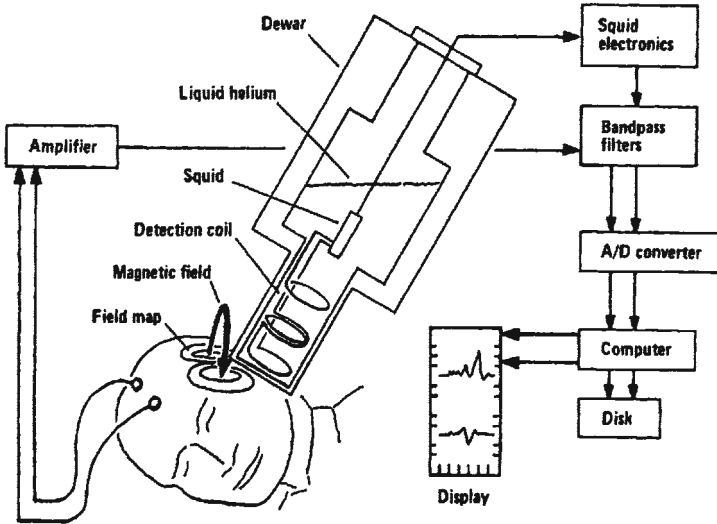


FIG. 1.3. Schematic of a single-channel neuromagnetometer measuring the brain's magnetic field. SQUID=superconducting quantum interference device.

in liquid helium, along with other components. The field emerging from and re-entering the skull is undistorted as it passes through the bottom of the tail section of the dewar.

In Fig. 1.3 the field from the brain is sensed by the bottom-most (detection) coil of a set of coils within the tail section of the dewar. The complete set of coils (sometimes referred to as a *flux transporter*) is composed of a superconducting material such as niobium, which, at very low temperatures, has no resistance at all to the flow of an electric current. This particular configuration of coils is referred to as a *second-order gradiometer*. Roughly this is how it works: Assume that we have a single coil of superconducting material in the dewar. If a magnet is nearby when liquid helium is poured over the coil (so that the loop enters the superconducting state), a current will continue to flow in the coil even after the magnet is removed. This current traps the enclosed magnetic flux (*the Meisner effect*). When the external magnetic field is changed, the current changes as well, to keep the trapped flux constant. Hence, the single coil may function as a *magnetometer* in the sense that monitoring the current flow is equivalent to measuring the applied magnetic field. However, since the magnetometer measures field per se, it is

affected by fields from distant as well as nearby sources. The multiple coils shown in Fig. 1.3 are wound in series with each other and also act to keep the trapped flux constant. However, this configuration is relatively insensitive to changes in fields from distant sources.

When a field is stronger near the bottom-most detection coil, the current flow will change in the entire gradiometer. In this case the detection coil is wound clockwise, while the next higher coil is wound counterclockwise. In fact, all adjacent coils are wound in opposition to each other. Thus, when placed in a uniform field the currents made to flow in these coils would cancel each other out. Because this gradiometer is composed of four loops (to form a *second-order gradiometer*), the application of a field with a uniform gradient would also result in self-cancellation of any effect. By contrast, the magnetometer (sometimes referred to as a *zero-order gradiometer*) responds to both uniform fields and fields with uniform spatial gradients. Fields of distant sources tend to have uniform spatial gradients. However, a nonuniform field (one with high spatial derivatives, as shown in the figure) has a stronger effect on the bottom-most coil, and this leads to a net change in current flow within the entire gradiometer.

This property of second-order gradiometers makes them relatively insensitive to fields associated with distant sources. In effect, the operation of a gradiometer (as opposed to a simple *magnetometer*, which is composed of a single coil of superconducting material) is analogous to the common-mode rejection of noise that is made possible by bipolar electrodes in EEG recordings. A *third-order gradiometer*, which is composed of even more coils, is even less sensitive to uniform fields as well as fields with moderate spatial gradients. In fact, a well-balanced second- or third-order gradiometer makes it possible to measure weak neuromagnetic fields in many unshielded environments despite the presence of ambient magnetic fields (see chap. 7). However, to gain maximum sensitivity to signals of interest, for some purposes the dewar and the human subject or patient are usually placed within a magnetically shielded room.

The SQUID never “sees” the external field it is trying to measure. It is isolated within a superconducting shield inside the dewar, effectively isolating it from the environment. However, the gradiometer includes a very small *signal coil* wound in series with all of the other coils. Unlike the other coils, the signal coil is located inside the superconducting shield along with the SQUID. In fact, the only contact the SQUID has with the outside world is through the signal coil. Whenever a field is applied to the detection coil so that current flows throughout the gradiometer, the SQUID detects the current

flowing in the signal coil, because that current is accompanied by its own magnetic field.

To describe this in more detail would distract us from our main objective. It suffices to say that the detection coils “sense” the magnetic field near the scalp, the signal coils “transmit” the currents in the detection coils to the SQUID, and the SQUID “converts” the currents in the signal coils to voltages that can be amplified and recorded by conventional electronic devices. The voltages are directly proportional to the magnetic field strength near the scalp. The single-channel system described here is based on the system designed and constructed by Brenner, Williamson, and Kaufman (1975) and used to detect the first evoked neuromagnetic field in an unshielded environment. However, as intimated earlier, this has been superseded by systems containing 200 or more SQUIDS. Also, the SQUIDS in use today are far more sensitive than the original SQUID and may be used with very different gradiometer configurations. For example, a gradiometer composed of several superconducting coils in a single plane may be used to sample differences in the radial field across the surface of the scalp. Such a configuration is described in some detail in chapter 9. Also, today sophisticated software is used to process signals from simple magnetometers to emulate different gradiometer configurations. Various whole-head systems are described in chapters 7–9.

Measuring the field at many places simultaneously permits identification of sources of neuromagnetic fields within the brain, thus overcoming one major problem. Early investigators had to assume that the source does not change from one measurement to another as a single-channel system is moved to sample the field at many different positions above the scalp. It is no longer necessary to make such an assumption.

EVENT-RELATED BRAIN ACTIVITY

It is obvious that the signals actually detected by neuromagnetometers are not produced by isolated current dipoles floating around in conducting solutions within spherical heads. However, in keeping with the didactic motive of this chapter, we approach more realistic situations slowly and in the process show why an elementaristic approach using spherical head models and point current dipoles has real value. We begin by considering Fig. 1.4.

It has been known for many years that activity in the brain stem may be evoked by acoustic stimuli and picked up by scalp electrodes. The extremely weak auditory brain stem evoked responses begin to appear about 2 msec after

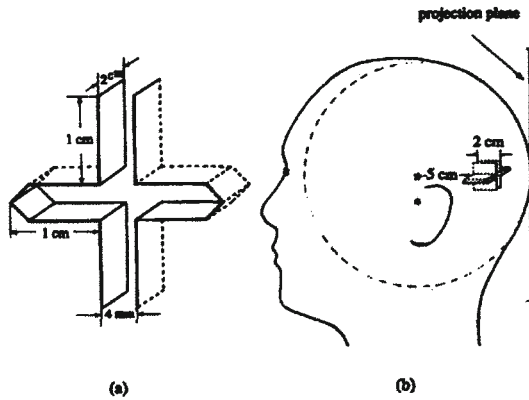


FIG. 1.4. Cruciform model of the visual cortex.

the onset of stimulation and run their courses before much stronger responses of the auditory cortex are picked up. On occasion, the latter are seen after a single stimulus event and are certainly strong enough to be detected reliably after averaging a few dozen trials. However; the brain stem activity must be averaged over several thousand trials to be detected. With the exception of this type of brain stem activity most brain activity seen in the EEG or the MEG originates in the dendrites of cells of the cerebral cortex—in the gray matter of the brain (see chap. 12 for examples of signals that may well be attributable to fields associated with spike potentials). As we shall see, this is enormously helpful in determining the approximate location in the brain of the sources of observed evoked magnetic fields.

The cortex of each hemisphere may be thought of as a two-dimensional but highly rumpled (convoluted) sheet of neural tissue. Although it is about 2 mm thick, this thickness is negligible when fields are measured at a distance. It is useful to think of this two-dimensional sheet as populated by a very large number of dipolar sources, all oriented normal to its surface. (We conducted computer simulations in which the individual dipoles of a large array are randomly tilted by as much as 45° from the normal. The summed isofield contours describing the radial component of magnetic fields at the surface of a spherical skull are essentially the same as when all of the dipoles are normal to the surface.) Of course, the dipoles represent aggregates of cells.

The cerebral cortex contains approximately 10 billion cells. Even if the cells were independent of each other, on occasion, by chance alone, ionic

currents within significant numbers of them would flow in the same direction at the same time. We refer to this as *synchronization*. In many instances this synchronization is initiated by some external or internal event. Where the initiating external event is a sensory stimulus—for example, a flash of light—we refer to a *sensory-evoked response*. Where the sensory stimulus results in the flow of current within a sufficient number of neighboring columns of cells within the same window of time (the activity need not start or end at precisely the same time), then it may be possible to pick up either an evoked potential or an evoked field. It has been estimated that something on the order of 100,000 concurrently active cells may be sufficient to produce a detectable extracranial neuromagnetic field. The visual cortex is a useful example. The central 2° of the retina (the *fovea*) is known to affect roughly 25% of the entire primary visual cortex (Brodmann's area 17). It is worth noting that the diameter of the entire fovea corresponds to a ~ 0.5-mm diameter image of a disk on the retina. This small patch of light centered on the retina could affect much of the occipital pole as well as a large area extending deeply into the longitudinal fissure, including the calcarine fissure. If the same small patch of light were moved away from the fovea and into the peripheral visual field, it would affect a very rapidly decreasing proportion of the cortex extending into the longitudinal fissure. The shape of the visual cortex is schematized in Fig. 1.4. This crosslike shape is sometimes referred to as the *cruciform model* of visual cortex. The calcarine fissure represents the arms of the cross, and the longitudinal fissure is the space between the two halves of the cross. Real brains lack this degree of symmetry, but the model is useful in several respects. First, it helps in explaining the retinotopic organization of the visual cortex and, second, it clearly illustrates how the shape of the brain might affect its observed neuromagnetic field.

Figure 1.5 illustrates how different regions of the visual cortex are excited when appropriate stimuli are placed in different quadrants of the visual field. The neurons of the cerebral cortex are arranged in columns oriented normally to its surface, so activation of the lower left quadrant of the cruciform model must result in a net flow of current either inward (away from the surface) or outward. Thus, it is possible to activate a rather large area of the cortex merely by presenting a moving or flashing pattern in an appropriate retinal location. The vast majority of columns of cells in these activated areas may be conducting current in the same direction at more or less the same time. Intuitively, this source of evoked activity is a far cry from a point current dipole.

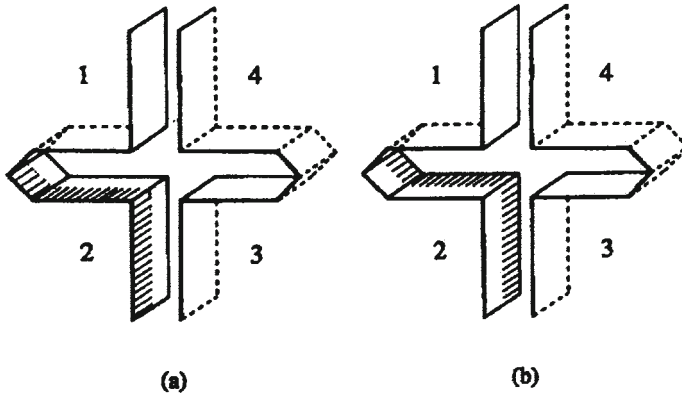


FIG. 1.5. A simulation in which the upper right quadrant of the visual field activates cortical cells of the lower left quadrant of the cruciform visual cortex. The shaded region in Panel (a) lies closer to the occipital pole and illustrates a possible distribution of activity evoked by stimulation in the upper right quadrant of the fovea. As the stimulus is moved away from the fovea and farther into the peripheral field, the depth of activity along the cortex shifts inward, as indicated by the greater depth of activity signified by the shaded area of Panel (b). The dipoles (columns of cells) in the shaded areas are oriented normal to the surface of the cortex.

The unshaded areas of cortex are also active. The cells in the unshaded areas are synchronized with each other by chance alone. For our purposes we may assume that the columns of cells filling the unshaded regions are randomly active; that is, the direction and magnitude of net current flow in one column cannot be predicted from that of its near neighbors. In point of fact, at any instant of time this random activity effectively masks the more coherent activity of the columns within the shaded areas. This explains why *signal averaging*, or some other method for enhancing signals relative to “noise,” is needed to recover evoked fields and potentials.

Kaufman, Kaufman, and Wang (1991) computed the isofield patterns associated with synchronized activation within the shaded areas shown in Fig. 1.5. Specifically they assumed that the shaded areas covered many dipoles, all oriented normal to the shaded surface. The only difference between Fig. 1.5a and Fig. 1.5b is that the shaded area in the latter is 1 cm deeper than the similar shaded area of Fig. 1.5a. The magnitudes of these dipoles were randomized, but their directions were the same, signifying that they are all synchronized with each other. In this simulation the large unshaded areas of the entire cruciform cortex were populated by unsynchronized dipoles, that is, dipoles whose moments were all randomized. On average, the magnitude

of current flowing in the synchronized dipoles was the same as that in the unsynchronized dipoles, although different values were selected at random every time the field at the surface of the skull was sampled. Overall, in this simulation the cruciform cortex was populated with 1,386 current dipoles. By superposition, the radial component of the field at the surface of the spherical head due to all of the dipoles was computed at 841 points, and these were plotted to form the isofield contour plots projected onto a plane. Several such plots are shown in Fig. 1.6. One hundred plots were computed to illustrate how the pattern of isofield contours changes because of random contributions by the asynchronous dipoles.

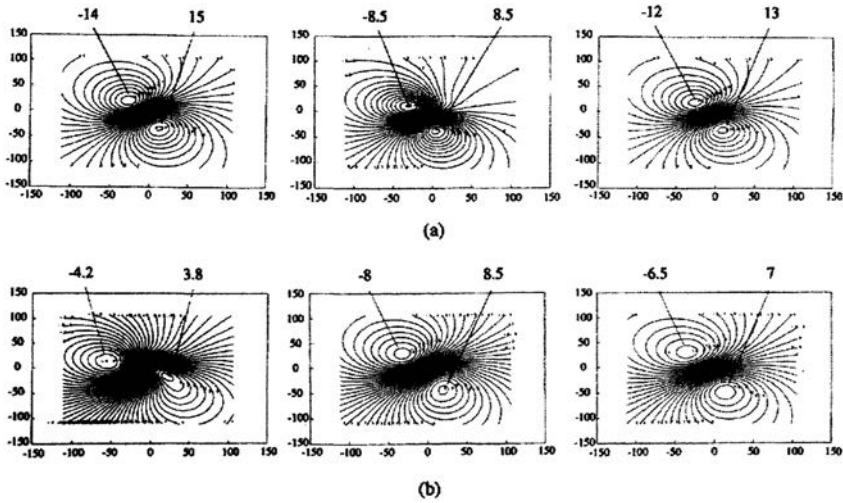


FIG. 1.6. Isofield contour plots associated with activation of a large number of current dipoles oriented normal to the surface of the cruciform cortex. The three plots in the upper row (Panel [a]) of the figure are based on synchronized activity in the outermost shaded area illustrated in Fig. 1.5. The two plots on the left side of (a) were selected at random from 100 such plots, where each corresponds to a different set of dipole moments. These 100 plots were averaged to produce the third plot on the right of (a). Note that the average values of the field extrema in this plot differ in magnitude from the two to its left. Also, the plots on the left are not as symmetrical as the average plot. The latter is best fit by the field that would be produced by a single equivalent current dipole. The relatively asymmetrical patterns on the left reflect contributions of dipoles dwelling in the unshaded portions of the cortex. Some subset of these dipoles would be synchronized with the evoking stimulus by chance alone. The three lower plots (Panel [b]) are based on synchronization of the (1-cm) deeper shaded area of Fig. 1.5b. Here, too, the single “trial” plots to the left are asymmetrical and differ in orientation and magnitude from each other and from the average plot on the right. Note that the space separating the average field extrema in (b) is wider than that of the righthand plot of (a).

The asymmetries of the two lefthand isofield contour plots in Fig. 1.6a and Fig. 1.6b are due to random contributions by the dipoles that populate the unshaded walls of the cruciform cortex. These asymmetries cannot be accounted for by assuming that a single current dipole underlies the observed field. Instead, a much better fit is achieved when one assumes that multiple dipoles contribute to the field. However, this pattern changes from one set of measurements to another. Averaging sharply reduces this variability, because the randomly varying moments of the dipoles that populate the unshaded regions tend to be self-canceling when their fields are averaged, and the resulting plot is a much closer fit to the pattern that would be produced by a single equivalent current dipole. Hence, a field pattern produced by hundreds or even thousands of dipoles can easily be confused with a pattern produced by a single equivalent current dipole.

Comments on Signal Averaging

Readers who are familiar with signal averaging may choose to skip this section, but several of its passages may prove to be worth scanning. Some subtle and frequently overlooked assumptions underlie this simple procedure for recovering signals from noise, and it is good to keep them in mind. For example, if the so-called “signal” (the event-related response) is not independent of ongoing asynchronous activity of the brain, then averaging can lead one to discard important data along with the noise. This is quite relevant to our discussion of spontaneous brain activity.

Figure 1.6 provides a demonstration of the effects of signal averaging. Isofield contour plots similar to those shown in Fig. 1.6 can be thought of as instantaneous maps of the field obtained by many sensors at once. One hundred such maps were generated as follows: One hundred independent sets of random numbers were generated to represent the current dipole moments (directions of current flow and their magnitudes) of all the dipoles in the unshaded areas of Fig. 1.5. This is the region that is assumed to be unaffected by the presentation of a stimulus. Similarly, the dipoles under the shaded areas were also represented by 100 independent sets of random numbers, but these represent only their magnitudes, as the direction of current flow was the same for all of the dipoles. The commonality of direction of current flow in this region is assumed to be due to the action of a stimulus or event that has the effect of synchronizing the neurons within the shaded regions. All of these values were used to compute the fields represented by 100 different isofield contour maps, represented by the samples in Fig. 1.6.

The 100 contour maps derived from the more shallow shaded area were then averaged to create the plot on the upper right side of the figure. Similarly, another 100 maps were averaged to create the lower plot on the same side of the figure. This averaging process reveals a contour plot largely due to the synchronized activity of the neurons under the shaded patch of the cortex. The cortex is normally active, regardless of whether a stimulus is present. Therefore, a sensor placed above the occipital cortex will detect a magnetic field at all times. Because of the asynchronous activity of the neurons that contribute to this field, its direction and strength will be different from time to time. However, when the field is repeatedly measured at a fixed time after the presentation of a stimulus, the field due to asynchronous activity will tend to be self-canceling, whereas averaging will reveal the synchronized activity evoked by the stimulus. Activity time-locked to the stimulus will increase arithmetically with the number of samples taken, whereas the presumably Gaussian background noise (due to the asynchronous activity, instrumentation noise, and ambient noise) will increase only as the square root of the number of samples. Although in realistic situations the background noise on a single trial is much greater in magnitude than the evoked response, when a sufficient number of samples enter the average, the evoked response ultimately becomes significantly larger in amplitude than the noise. All of this assumes that the noise is independent of the evoked response. Much of the literature tacitly assumes that a change in voltage or field that is time locked to the evoking event is the only relevant consequence of stimulation. As we shall see, this assumption is often invalid.

Are Event-Related Voltages and Fields Independent of Brain Noise?

The logic underlying this section is quite simple. We begin by assuming that neural tissue is active regardless of whether a particular external stimulus is presented. The activity may be due to intrinsic biochemical changes, activity originating in the thalamus and transmitted to the cortex, or any of several possible conditions. The external stimulus, on reaching the cortex, may well interrupt or alter this ongoing activity. Hence, if the stimulus causes the current flow within a neuronal population to be synchronized, it may also either add to (or subtract from) the ongoing activity. If the evoked activity merely adds linearly to the ongoing activity, then, in effect, it is independent of that activity, and the time-locked response is the only consequence of stimulation. However, if the level of activity of the affected neurons is not the linear sum

of the ongoing activity and of the evoked activity, then consequences of stimulation may not be detectable in the averaged response.

Linear and Nonlinear Systems. Any system, whether it is an electronic circuit or a portion of the nervous system, can be described as being either a *linear system* or as a *nonlinear system*. If two signals are applied concurrently to a linear system, the output of that system is equal to the sum of the outputs of the same system to the same inputs presented at different times. In this case, we say that the *superposition principle* applies to the system. When the superposition principle does not apply, we say that the system is nonlinear.

If a sinusoidally varying signal is applied to a linear system, then its output will be a sinusoid at the same frequency as the input. Although the amplitude of the output may not be uniform for inputs of different frequency a linear system always responds at the same frequency as that of the input. It has been known for some time that visual responses evoked by sinusoidally modulated light often occur at twice the frequency of the stimulus. Any system that responds to an input of one frequency with an output of another frequency is necessarily nonlinear.

Figure 1.7 explains how frequency doubling occurs in the case of one nonlinear system. In this case; the output of the system is the square of the input. (The same is true if the output is proportional to the square of the input, except that the proportionality constant defines the amplification afforded by the system.) Thus, where the input is $a \sin \omega t$, the output

$$Y_{\text{output}} = (a^2 \sin^2 \omega t). \quad (1.3)$$

From elementary trigonometry,

$$A^2 \sin^2 \omega t = a/2 - a/2 \cos 2\omega t. \quad (1.4)$$

As in Fig. 1.7, this demonstrates that, when squared by a nonlinear system, a sinusoidal input (frequency= ωt) amplitude a results in an output at twice the frequency of the input ($2\omega t$) and one half the amplitude of that frequency. Furthermore, the output has a Fourier component which, in this case, has an amplitude $a/2$ and a frequency of zero (a *dc* component).

Squaring is not the only form of nonlinearity. For example, many biological systems transform an input stimulus so that the response of the system is approximately proportional to the logarithm of the stimulus.

The output of such a system to a sinusoidal signal oscillating about an

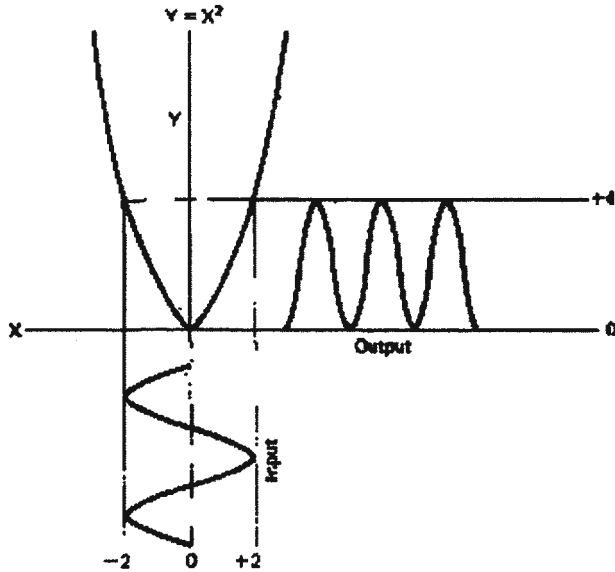


FIG. 1.7. Effect of applying a sine wave (input) to a device whose output is the square of the input. The graph represents the equation $Y=X^2$. Note that the sinusoidal input has a mean value of zero and, in arbitrary units, its amplitude peaks at 2 and -2 . The output amplitude peaks at 4 and 0, so it happens to be the same (4 units) as that of the input. However, the average of the squared output is one half the peak-to-peak amplitude, and the output contains a sine wave.

average value of zero (as in Fig. 1.8) contains a *dc* offset and odd harmonics of the frequency of the input. Similarly, systems that clip the smoothly varying positive and negative peaks of sine wave inputs also generate odd harmonics.

Half-wave rectifiers are sometimes referred to as *linear rectifiers*. These are not linear at all; rather, their outputs represent only the positive (or negative) peaks of sinusoidal inputs, and these too contain odd harmonics of the input. In general, the relative amplitudes of these harmonics depend on the nature of the nonlinearity and on whether the input signal is a simple sine wave or if it can be represented as the modulation of a steady *dc* signal. In fact, if the *dc* component of the input is large relative to its sinusoidal modulation, the effect of the existing nonlinearity may become negligible. Incidentally, this is one of the main reasons why researchers studying the response of the visual system to sinusoidally modulated light may use a near-threshold degree of

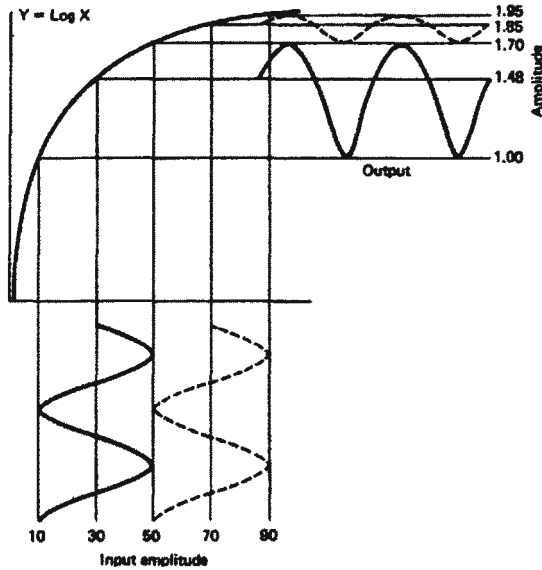


FIG. 1.8. The output of this nonlinear system is proportional to the logarithm of its input. As demonstrated here, a sinusoidal input is distorted by the system so that its output is not a pure sine wave. In this case the distortion is most obvious when the input is low (solid line) and less obvious when the input rides on a high *dc* (dashed line). This is one reason why vision researchers superimpose a sinusoidal variation in light level on a *dc* “pedestal.”

modulation of a steady light as a stimulus. Despite its inherent nonlinearity, when presented with such a stimulus the visual system is approximately linear in its behavior. It is said that real eyes evolved to deal with large-scale changes in visual stimulation, so allowing for effects of nearly pervasive nonlinearity is essential to understanding the perceptual process.

Nonlinearities exemplified by different kinds of rectification—for example, square law—have quite different effects from those attributable to saturation, for example, when a sensory stimulus is so intense that an otherwise linear system ceases to respond to additional increases in its intensity. We do not consider such effects here except to say that in some evoked-response experiments investigators fail to use a range of stimulus intensities—for example, contrast or loudness—that include very low values as well as high ones. This is the only way to determine if the observed responses are influenced by saturation nonlinearities rather than some other ostensible cause.

Interactions of Signals at Different Frequencies. Thus far we have not dealt directly with the interaction between the response of the brain and its ongoing activity. It is easier to understand how such an interaction may come about by describing what happens when two signals of different frequencies are applied concurrently to the same nonlinear system. As stated earlier, in a linear system the response to concurrent stimuli is the same as sum of the responses to the two stimuli applied separately. It is extremely important to note that even if the brain as a whole were essentially nonlinear, if the two stimuli were to affect different regions so that no interaction is possible, then the response would also be the same as the sum of the responses to the two stimuli when applied separately. In chapter 5, Regan and Regan exploit this distinction to gain insight into how signals are parsed by the sensory systems. For now we deal only with the case where two different signals are applied concurrently to the same nonlinear system.

Suppose that lights are modulated at two different frequencies, and the frequency of one is not a harmonic of the other. For example, one light is modulated at 7 Hz and the other at 10 Hz. Both lights are imaged in the same place on the retina. When a signal-averaging computer is time locked to a signal at 7 Hz, then a response is usually recovered at that frequency or, on occasion, at its second harmonic, that is, 14 Hz. Similarly when time locked to the concurrently presented 10-Hz stimulus, a response is recovered at 10 Hz and at its second harmonic, that is, 20 Hz. It is interesting to note that when the 7-Hz and 10-Hz signals that drive the two stimuli are multiplied, the output of the multiplier does not contain signals at either 10 Hz or 7 Hz. Rather, the output is at 3 Hz (the difference between 7 and 10 Hz—the so-called *difference frequency*) and at 17 Hz (the *sum frequency*). If the output of the multiplier were applied to a signal-averaging computer time locked to either of the original 7- and 10-Hz inputs to the multiplier, the averaging computer would reveal no signals whatsoever. This is because the sum and difference frequencies are not integer multiples of 7 or 10 Hz. Now suppose that when the two stimuli are presented to a subject, some of the affected portions of the nervous system are nonlinear. The result is that the nonlinearities produce sum and difference frequencies, and these cannot be recovered when a signal averager is time locked to either stimulus. It is of some interest to note that Helmholtz (1885/1954) postulated the presence of nonlinearities in the auditory system to account for the so-called *combination tones*. These are perceived when a listener is presented with two different pure tones far enough apart in frequency so that one does not hear ordinary beats. In chapter 5, Regan and Regan describe several kinds of nonlinearity

and how it results in the generation of frequencies that are not harmonics of concurrently applied stimuli. Taken together, the bands of frequencies generated by nonlinear interactions are referred to as *sidebands*. Using a very sensitive spectrum analyzer rather than an averaging computer, Regan and Regan were able to discern the presence of sidebands when the subject is stimulated and their absence without stimulation. These sidebands do not contain components that are harmonics of the applied stimuli. As Regan and Regan point out, this information may be invisible to the averaging computer, but it can still be retrieved and used to gain insights into the nature of neural processes underlying sensory phenomena. For example, detecting frequency components that are a consequence of stimulation but are unrelated harmonically to the stimuli is a powerful way to determine where in the brain inputs from different sense modalities produce effects that interact with each other.

We now illustrate this point with a hypothetical experiment. Suppose that a periodic visual stimulus is presented to the eyes and that periodic acoustic stimuli are presented to the ears. If the two types of stimuli are not harmonics of each other, then an averaging computer can easily detect the separate and independent responses they evoke in the visual and auditory parts of the brain. Regan and Regan (1987) used this approach to determine whether independent channels exist within single-sense modalities, for example. In our hypothetical experiment one can set the sweep duration of the averaging computer so that it corresponds to the period of the visual stimulus and then to the period of the acoustic stimulus. The visual and auditory responses would emerge from the background noise. If the neural effects of these stimuli should interact with each other, then a high-resolution spectrum analysis can reveal the presence of the products of the interaction, that is, sidebands. By mapping the fields about the scalp that fluctuate in step with frequency components of the sidebands, it is possible to locate the regions of the brain in which the interactions occur, as these regions may be represented as current dipoles. This appears to be a very promising line of research that should be pursued by researchers working in EEG as well as in magnetic source imaging (MSI).

In this chapter, however, our concern is less with the sidebands generated by concurrently presented stimuli than with the question of the independence (superimposability) of effects of sensory stimuli and the ongoing activity of the brain. However, the same basic principles apply.

Models of cortical circuits may incorporate extracortical oscillators that lead to apparently spontaneous changes in neuronal membrane potentials. So, for example, signals originating in the brain stem activate cortical neurons

at the frequencies of the alpha rhythms. Similarly, when a sensory stimulus is applied to the organism; signals travel along thalamocortical pathways to evoke cortical activity. These evoked responses may well interact in the cortical neurons with the effects of signals from the hypothetical extracortical oscillators. In this case the evoked response would modulate the so-called “spontaneous activity” of the affected cortical neurons (Kaufman & Locker, 1970).

Cross-Modulation of Evoked Response and Spontaneous Brain Activity.

When a response evoked at one frequency interacts with a concurrent response evoked at some other frequency one says that each response modulates the other. In fact, this is precisely what happens when an electric signal at acoustic frequencies is used to modulate another electric signal at a radio frequency to produce an amplitude-modulated wave for radio transmission. The modulated wave is composed of the original radio frequency signal plus sidebands composed of the sums and differences of the original acoustic signal and the radio frequency signal. By contrast, ongoing brain activity is not a spectrum of discrete frequency components; rather, the spectrum is continuous. As a result, the sidebands are not composed of discrete spectral lines. They too, form a continuous spectrum. Despite this difference, we shall see that the ongoing activity of the brain can be altered or modulated in amplitude when a response is evoked by a sensory stimulus.

The presence of this modulation is proof of two things: first, that the brain responds in a nonlinear manner to incoming signals, and second, that the measured activity of the brain is not independent of the so-called noise represented by the brain’s spontaneous activity.

Hans Berger, the discoverer of the EEG, also discovered a phenomenon he described as *alpha blockage*. A frequency band ranging from about 8 Hz to 12 Hz predominates in the EEG measured over the occipital region of the brain. This is the so-called *alpha band*. It is strongest when the subject is resting with eyes closed and diminishes dramatically if subjects open their eyes and become alert and attentive. During this state of alpha blockage the EEG is dominated by activity in a band around 20 Hz or, roughly, twice the alpha frequency. This so-called *beta* activity is weaker in amplitude than the alpha activity it purportedly replaces. It should be noted that activity at roughly 8 Hz to 12 Hz tends to be predominant over most of the scalp, but when it appears to arise in the region of motor cortex it is referred to as *mu* activity. For the purposes of this chapter we refer to all activity in this frequency band as alpha. In any event, an early and still widely accepted

theory is that activity in the alpha band is due to the synchronization of many cortical neurons whose electric fields tend to oscillate at a frequency in a band surrounding 10 Hz. According to this theory, the replacement of alpha by beta is due to the desynchronization of the neurons, which occurs when the neurons are activated. The ostensible desynchronization implies that the individual neurons still oscillate at alpha frequencies, but the fields of these neurons tend to be self-canceling when they are out of step with each other. So, according to this view, the lesser energy detectable at beta frequencies really means that the neurons are more active, rather than less active, during alpha blockage. On the basis of this, one can claim that alpha blockage is not due to a suppression of alpha activity that goes on independently of any other activity in which the neurons might become engaged. However, when otherwise engaged, the neurons are no longer idling along in a synchronous fashion. Hence, by this theory, the signal (which results in activation) is independent of the noise. However, evidence suggests that this view may not apply

It seems likely that event-related or -evoked activity modulates ongoing activity of the brain, which implies that the evoked response is not independent of the so-called noise. We should also note that computer simulations of a sheet of asynchronous dipoles oriented normally to the surface of the walls of a sulcus show that more field power may be produced when the dipoles are synchronized than when they are desynchronized (Kaufman et al., 1991). This depends on the geometry of the cortex, especially its symmetry. In the EEG domain, synchronized dipoles located in the gyrus may actually produce higher voltages at the scalp than when they are asynchronous. In any event, it is far from proven that alpha blockage is due solely to desynchronization; it may also be due to some kind interaction of event-related activity and spontaneous activity

Measuring the Interaction. One way to determine whether evoked activity interacts with spontaneous activity is to examine the entire frequency spectrum of the brain's magnetic or electric fields. This could reveal that energy is added at frequencies that are not harmonics of the fundamental frequency of the stimulus. During signal averaging such frequency components would be discarded along with noise. Thus far, little research has used this straightforward approach. However, an indirect method has revealed the presence of modulation of brain activity by event-related activity.

Kaufman and Price (1967) developed this indirect method to examine high-frequency cortical activity (300 Hz-1000 Hz) associated with visual stimulation. This is the same band of activity that Hashimoto discusses in

chapter 12. Kaufman and Price recognized that a 1-msec pulse (as in the action potential) has a frequency spectrum containing energy at frequencies ranging from *dc* to about 1 kHz. As it happens, the frequency spectrum of a single impulse is essentially the same as that of an infinite number of randomly occurring identical impulses. Therefore, if a large number of impulses occur in a more or less random sequence across many neurons within the same interval of time, it is theoretically possible to detect activity at frequencies well above the range of the normal EEG (*dc* \sim 60 Hz) with scalp electrodes. The stimulus was a light flashing at 15 Hz. The output of a wide-band amplifier measured the voltage across two scalp electrodes over the occipital cortex. The output of the amplifier was filtered to pass activity between 300 Hz and 1000 Hz. This activity was then squared (rectified) and applied to a low-pass filter. A lock-in amplifier was used to detect activity in the rectified EEG at 15 Hz that was time locked to the stimulus. The presence of such activity would indicate that the high-frequency band was modulated by evoked activity at the frequency of the stimulus. A statistically significant response was found. This indicated that visual stimulation resulted not only in an evoked response at the frequency of the stimulus but also in side bands that were not harmonics of the stimulus. These side bands happened to be in the high-frequency domain. Essentially this same method has revealed that activity in the low-frequency band of the normal EEG and MEG is also modulated by sensory stimulation and other events.

Assuming that a 15-Hz visual stimulus does not evoke responses containing harmonics above 150 Hz, the responses detected after squaring the 300 Hz-1 KHz band can be thought of as the variance about a mean zero response. (Actually assuming them to be present, Kaufman and Price [1967] undertook to remove such high harmonics, and the remaining noise was still modulated at 15 Hz.) Kaufman and Locker (1970) used this same procedure to demonstrate a similar modulation of harmonically unrelated activity within the normal EEG band by a visual stimulus.

The variance about a mean response of zero is proportional to *power*. Voltage is often expressed in terms of *rms* (root mean square) volts. It should be noted that *rms* voltage is mathematically identical to the *familiar standard deviation* of statistics, which, in turn, is the square root of variance. Hence, *electric power* is the same as variance (voltage squared), whereas *field power* is equivalent to field squared. Several studies have revealed that MEG and EEG power fluctuate during the performance of several different cognitive tasks, for example, memory search for tones and for visual forms, as well as during a mental rotation task (Kaufman, Curtis, Wang, & Williamson, 1991;

Kaufman, Schwartz, Salustri, & Williamson, 1990; Michel, Kaufman, & Williamson, 1993; Rojas, Teale, Sheeder, & Reite, 2000). In these studies it was found that the duration of a profoundly reduced level of alpha power was highly correlated with time to scan memory for tones or forms as well as to signal completion of a mental rotation task. The distribution of affected field power across the scalp appeared to differ with the modality involved, and was therefore not a generalized effect of, for example, heightened alertness. The affected activity is not synchronized with any stimulus event, although the modulation of its power is related to the time required to perform the task. ERP and event-related field (ERF) studies of short-term memory search and many other cognitive tasks reveal differences in amplitude of various response components, but in most studies these are not as well correlated with the time required to complete the task.

It is clear that background activity is affected by stimulation and by performance of cognitive tasks. These effects are not mirrored in the standard ERP or ERF. Hence, this is an area that should be explored more extensively. For the present it suffices to stress the following point: The so-called noise rejected during signal averaging may well contain significant information related to sensory responses and cognitive processes. This could involve specific regions of the cortex, depending on the modality and the nature of the task. One way to begin to study the relation between this information and mental processes is simply to compute the variance within different frequency bands about the average response. This is well within the capabilities of modern desktop computers, so researchers no longer need to rely solely on differences between average responses both within and across subjects, which is the traditional way to study response reliability and its inverse, variability.

LOCATING THE SOURCE

One of the ostensible advantages of MEG is that the radial neuromagnetic field is not distorted by the intervening bone, skin, and other tissues. Hence, in principle it should be simpler to locate the source of the observed field than it is to do so on the basis of EEG measures. Because evidence suggests that spontaneous activity originating in specific regions of the cortex may be differentially affected by cognitive tasks, it is of some interest to inquire as to how well one might locate those regions on the basis of field or field power data. Wang and Kaufman deal with this particular issue in some detail in chapter 4. We shall briefly introduce the same topic here, beginning with the

much simpler problem of locating the source of a neuromagnetic field when that source is modeled as an equivalent current dipole.

The Problem With the Inverse Problem

Brenner; Lipton, Kaufman, and Williamson (1978) stimulated the little finger of one hand with a periodic electric impulse. This evoked a neuromagnetic field in a confined region over the hemisphere contralateral to the stimulated finger. The investigators measured the radial field at many places across the scalp. The same stimulus was applied to the thumb of the same hand, and the field pattern was measured again. As expected, the field pattern associated with the stimulation of the little finger contained a region where the field was directed outward from the head and, at the same time after stimulation, another region where the field was directed inward. The same polarity reversal of the field pattern was associated with the stimulation of the thumb, but one important difference was evident in the empirical isofield contour plots: The field extrema associated with stimulation of the little finger were about 2 cm lower on the scalp than those associated with stimulation of the thumb. Furthermore, these field extrema were located approximately above the projection of the central sulcus onto the scalp. The source of activity evoked by stimulation of the little finger is located along the posterior bank of the central sulcus and about 2 cm lower down than the source of activity evoked by stimulation of the thumb. This was probably the first empirical evidence that it is possible to identify the locations of current dipole sources on the human cerebral cortex, and it led directly to many studies in which ECD localization was based on neuromagnetic field measurements. As Wang and Kaufman discuss in chapter 4, it is possible to compute the field everywhere outside a sphere filled with a conducting fluid and containing a current dipole of a given strength, orientation, and position. One, and only one, field pattern can be attributed to this dipole. Hence, one says that there is a unique solution to the so-called *forward problem*. However, it is not possible to determine the strength, orientation, and position of a current dipole solely on the basis of the observed external field. This follows from the fact that any number of dipole s or combinations of dipoles could produce the same field. When one considers that all actual measurements are accompanied by noise, the uncertainty surrounding the validity of any putative source of the observed field is even greater. Even without this uncertainty, in principle it is impossible to discover a unique solution to the so-called *inverse problem*.

Investigators attempting to identify sources of observed field patterns (such as those associated with the little finger and thumb) resort to different strategies. We do not consider all of them here, but most begin with an informed guess as to the location of the source, for example, normal to the posterior bank of the central sulcus when studying responses to stimulation of a finger. Computer simulations may be used in which a current dipole is placed at a particular location in a sphere that best fits the subject's head, isofield contours plotted on the basis of solutions to the forward problem using Equations 1.1 and 1.2. The fit of these contours to those that were actually observed is tested. The moment, depth; and orientation of the dipole is then altered in an iterative fashion until a best fit (in the least squares sense) is achieved. The computed position of the dipole is then plotted in a magnetic resonance imaging scan. A similar procedure may be used when dealing with pathological states in which particular waveforms recur with some frequency (e.g., interictal spikes in the MEGs of some epileptics). When the computed positions of ostensible dipole sources are plotted in magnetic resonance imaging scans of such patients, the ECDs are often found to be in or near observable lesions. In some cases the lesions cannot be visualized, but surgical procedures have revealed small tumors near the computed sites of the ECDs.

A single equivalent current dipole may well account for an observed field pattern, and, when noise is relatively low, one might achieve an even better fit by assuming contributions of quadrupolar and possibly higher order sources. This alone is a useful but relatively modest accomplishment when compared with a larger goal of MSI. As we have taken pains to point out, the actual sources of observed fields are extended distributions of currents on the cerebral cortex. Many investigators have been tantalized by the possibility of finding a way to describe these extended distributions of current based on measurements of the brain's magnetic field. In chapter 4, Wang and Kaufman cite and briefly describe some of these efforts. They describe one such approach, the *minimum norm least squares* (MNLS) inverse, in some detail, along with results of computer simulations. The simulations were designed to demonstrate that there are circumstances in which it is entirely feasible to find a unique solution to the problem of describing the spatial distribution of currents on the cortex. Solutions to these inverse problems primarily require accurate knowledge of the geometry of the surface of the cortex and also assume that the elements of current that make up the distribution flow normal to the surface of the cortex. In principle, given a properly constrained problem, it is possible to arrive at a unique solution to the inverse problem of describing distributed current sources of observed magnetic fields. The